

## Accepted Manuscript

Configuration change from *cis* to *trans* of isothiocyanato groups in nickel(II) species: experimental verification and theoretical interpretation of reaction consequence and study on their bio-activity

Jaydeep Adhikary, Prateeti Chakraborty, Tanmay Chattopadhyay, Ritika Prasad, Yair Motro, Biplob Koch, Franz A. Mautner, Yifat Miller, Debasis Das

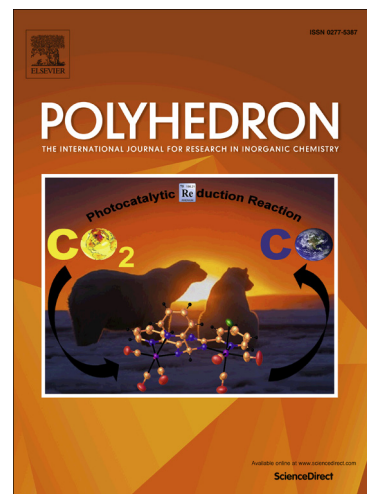
PII: S0277-5387(15)00168-0  
DOI: <http://dx.doi.org/10.1016/j.poly.2015.03.030>  
Reference: POLY 11253

To appear in: *Polyhedron*

Received Date: 9 December 2014  
Accepted Date: 19 March 2015

Please cite this article as: J. Adhikary, P. Chakraborty, T. Chattopadhyay, R. Prasad, Y. Motro, B. Koch, F.A. Mautner, Y. Miller, D. Das, Configuration change from *cis* to *trans* of isothiocyanato groups in nickel(II) species: experimental verification and theoretical interpretation of reaction consequence and study on their bio-activity, *Polyhedron* (2015), doi: <http://dx.doi.org/10.1016/j.poly.2015.03.030>

This is a PDF file of an unedited manuscript that has been accepted for publication. As a service to our customers we are providing this early version of the manuscript. The manuscript will undergo copyediting, typesetting, and review of the resulting proof before it is published in its final form. Please note that during the production process errors may be discovered which could affect the content, and all legal disclaimers that apply to the journal pertain.



**Configuration change from *cis* to *trans* of isothiocyanato groups in nickel(II) species: experimental verification and theoretical interpretation of reaction consequence and study on their bio-activity**

Jaydeep Adhikary,<sup>a</sup> Prateeti Chakraborty,<sup>a</sup> Tanmay Chattopadhyay,<sup>b</sup> Ritika Prasad,<sup>c</sup> Yair Motro,<sup>d,e</sup> Biplob Koch,<sup>\*c</sup> Franz A. Mautner,<sup>\*f</sup> Yifat Miller,<sup>\*d,e</sup> Debasis Das<sup>\*a</sup>

<sup>a</sup>*Department of Chemistry, University of Calcutta, 92 A. P. C. Road, Kolkata-700 009, India*

*E-mail: [dasdebasis2001@yahoo.com](mailto:dasdebasis2001@yahoo.com)*

<sup>b</sup>*Department of Chemistry, Panchakot Mahavidyalaya, Sarbari, Purulia, Pin-723121, India*

<sup>c</sup>*Department of Zoology, Faculty of Science, Banaras Hindu University, Varanasi-221005, U. P., India. E-mail: [kochbiplob@gmail.com](mailto:kochbiplob@gmail.com)*

<sup>d</sup>*Ilse Katz Institute for Nanoscale Science and Technology, Ben-Gurion University of the Negev, Be'er-Sheva 84105, Israel*

<sup>e</sup>*Department of Chemistry, Ben-Gurion University of the Negev, P.O. Box 653, Be'erSheva 84105, Israel. E-mail: [ymiller@bgu.ac.il](mailto:ymiller@bgu.ac.il)*

<sup>f</sup>*Institut fuer Physikalische und Theoretische Chemie, Technische Universitaet Graz, Austria*  
*E-mail: [mautner@tugraz.at](mailto:mautner@tugraz.at)*

**ABSTRACT**

Two new mononuclear Ni(II) complexes, namely [Ni(HL)(SCN)<sub>2</sub>(H<sub>2</sub>O)] (1) and [Ni(HL)(SCN)<sub>2</sub>(4,4'-bipy)] (2) [HL= 2-[(2-piperazin-1-yl-ethylimono)-methyl]phenol] have been synthesized and structurally characterized. The uncoordinated nitrogen atom of the piperazine moiety is protonated to provide electrical neutrality to the system. The configuration

of the isothiocyanato ligands is different in the two complexes, *cis* located in **1** and *trans* in complex **2**. The change of configuration of the isothiocyanato groups on addition of the neutral spacer 4,4'-bipyridine to complex **1** has been monitored by conductometric and FTIR spectral studies and the most probable mechanistic pathway has been proposed. DFT calculations have been performed and the outcome corroborates well with the experimental facts. The anticancer activity of the two Ni(II) complexes has been evaluated in human cervical (HeLa) cancer and breast cancer (MCF-7) cell lines. The cytotoxic effects of these complexes were determined by an MTT assay. The fluorescent intensity obtained in HeLa cells reveals the generation of ROS by the complexes using DCFH-DA (2,7-dichlorofluorescein diacetate) dye. The apoptotic cell death was determined by fluorescent staining with acridine orange and ethidium bromide, which confirmed the presence of apoptotic cells. Further, flow cytometry analysis was done, suggesting an arrest of the cell cycle in the S phase of the HeLa cells. Although a detailed molecular mechanism for the anticancer activity of the two complexes was not ascertained, the experimental results suggest that both complexes are effective anticancer agents, with complex **2** seeming to be more promising. The result also indicates that the apoptotic cell death in the cancer cell might be triggered by the process of ROS generation with the complexes. Thermogravimetric analysis of two complexes hints that NiO particles are the final product after decomposition of the complexes at 600 °C.

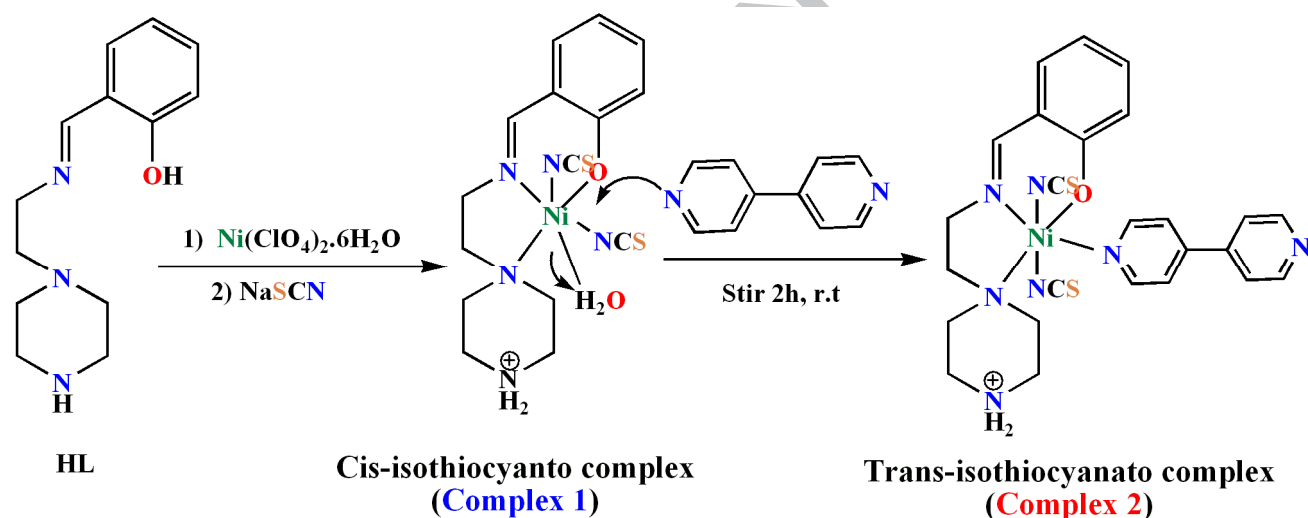
## 1. Introduction

Nickel is generally tagged as carcinogenic and toxic, not only in its metallic state but also in its complexed form, irrespective of its oxidation state. However, recent developments nullify this tag to some extent and establishes a possible therapeutic interest in some nickel-based

complexes [1-9]. Surprisingly the largest congener of nickel, i.e. platinum, has brought about a revolution in the field of medicine, in particularly in chemotherapy with the serendipitous discovery of the amazing anticancer activity of *cis*-platin, a purely inorganic compound. Interestingly, *trans*-platin has shown virtually no activity and thus establishes a myth that the configuration of the species may control the reactivity. It is well known to us that the coordination chemistry of Ni(II) is very fascinating owing to its inherent ability to adopt various coordination geometries, which often interconvert depending on certain factors, like the nature of the ligands, solvent, temperature etc [10-22], and thus as far as geometrical diversity is concerned Ni(II) may exhibit more diversity in its complexes compared to Pd(II)/Pt(II). It is well documented that the combination of isothiocyanate and nickel(II) in the presence of a diamine or a Schiff-base as a co-ligand may generate *cis*-/*trans* or linkage isomers or polymeric species [23-33]. It is also very interesting and challenging to convert one isomeric product to another or to convert the configuration of isothiocyanato ligands from *cis* to *trans* or vice versa. With those aims in mind, in the present study we have selected 2-[(2-piperazin-1-yl-ethylimino)-methyl]phenol (HL), a Schiff-base, as a co-ligand which on reaction with Ni(ClO<sub>4</sub>)<sub>2</sub> followed by NaSCN produces exclusively one product, namely [Ni(HL)(SCN)<sub>2</sub>(H<sub>2</sub>O)] (**1**) having two isothiocyanato groups in the *cis* position. Then we treated complex **1** with several neutral spacers and/or ligands like pyridine-N-oxide, imidazole, 2,2'-bipyridine, 4,4'-bipyridine etc. We were successful in making a new complex only when 4,4'-bipyridine was used and crystal structure analysis reveals that the configuration of the two isothiocyanato groups changes to *trans* (Scheme 1). The reaction pathways associated with the configurational change of the isothiocyanato groups have been established experimentally and rationalized by DFT

calculations. Here, it is noteworthy that even in the presence of excess of water complex **2** never reverts back to **1**, which has also been authenticated by DFT calculations.

The apparently diverse activity of the two geometrical isomers of  $\text{Pt}(\text{NH}_3)_2\text{Cl}_2$ , as stated above, inspired us to investigate the preliminary activity of our two complexes, having isothiocyanato ligands in *cis* and *trans* orientations, as antitumor agents. We have thoroughly investigated the cytotoxicity of our complexes on Hela and MCF-7 cells and explored the origin of the antitumor activity of our complexes where interestingly the *trans*-species shows slightly higher activity. Ultra-pure NiO was prepared using the pyrolytic decomposition of complexes **1** and **2** for 2 h, a technique used earlier [34,35].



Scheme 1. Synthetic route to complexes **1** and **2**.

## 2. Experimental

### 2.1. Materials and method

All the chemicals salicylaldehyde, N-(2-aminoethyl)piperazine, nickel(II) perchlorate hexahydrate, sodium thiocyanate and 4,4'-bipyridine were obtained from commercial sources

and used as received. All other chemicals are of AR grade. Solvents were dried according to standard procedures and distilled prior to use. Dulbecco's modified eagle medium (DMEM) was purchased from Cellclone, (Genetix Biotech Asia Pvt. Ltd.), Fetal bovine serum (FBS), 1000 IU of penicillin, 10 mg/mL streptomycin and the MTT reagent from Himedia, India. DMSO (dimethylsulphoxide) and RNase were obtained from GeNie, Merck, India. Ethidium bromide, Triton X-100 and other chemicals of analytical grade were purchased from Lobachemie Pvt. Ltd., India. Acridine orange was obtained from SRL Pvt. Ltd., India. Agarose and 2',7'-dichlorodihydrofluorescein diacetate (DCFH-DA) were purchased from Sigma, USA, whilst propidium iodide (PI) was obtained from EMD Millipore-Calbiochem, USA.

Elemental analyses (carbon, hydrogen and nitrogen) were performed using a Perkin-Elmer 240C analyzer. Infrared spectra ( $4000\text{-}400\text{ cm}^{-1}$ ) were recorded at  $28\text{ }^{\circ}\text{C}$  on a Shimadzu FTIR-8400S spectrophotometer using KBr as the medium. Electronic spectra ( $1400\text{-}200\text{ nm}$ ) were obtained at  $27\text{ }^{\circ}\text{C}$  using a Shimadzu UV-3101PC spectrophotometer with methanol and acetonitrile as the solvent and reference. The conductance of methanolic solutions of the complexes was measured using a SYSTRONICS 306 conductivity meter. Thermal analyses (TG-DTA) were carried out on a Mettler Toledo (TGA/SDTA 851) thermal analyzer in flowing nitrogen at a rate of  $30\text{ cm}^3\text{ min}^{-1}$ . X-ray powder diffraction (XRPD) was performed on a XPERT-PRO diffractometer with monochromated Cu-K $\alpha$  radiation (40.0 kV, 30.0 mA) at room temperature. Colorimetric analysis for the MTT was analyzed in a microplate reader Microscan (MS5608A). The fluorescence image analysis was done under a fluorescence microscope (Nikkon E800), whereas the cell cycle phase distribution was analyzed on FAC Scan machine (Becton Dickinson).

## 2.2. Synthesis

### 2.2.1. Preparation of $[Ni(HL)(SCN)_2(H_2O)]$ (**1**)

A methanolic solution (5 mL) of N-(2-aminoethyl)piperazine (0.258 g, 2 mmol) was added dropwise to a hot methanolic solution (10 mL) of salicylaldehyde (0.244 g, 2 mmol) and the resulting solution was refluxed for 1 h. The mixture was then cooled to room temperature. A methanolic solution (10 mL) of  $Ni(ClO_4)_2 \cdot 6H_2O$  (0.731 g, 2 mmol) was added to the Schiff base solution and the resulting solution was stirred for 3-4 h. The solution was then cooled, followed by the addition of an aqueous solution (5 mL) of NaSCN (0.324 g, 4 mmol). The solution was allowed to stir further for 2 h. The resulting green solution was filtered, kept in a  $CaCl_2$  desiccator in the dark and after a few days crystals suitable for X-ray data analysis were obtained. Yield 79%. *Anal.* Calc. for  $C_{15}H_{21}N_5O_2S_2Ni$ : C, 42.25; H, 4.92; N, 16.42. Found: C, 42.29; H, 4.98; N, 16.67%. IR (KBr,  $cm^{-1}$ ):  $\nu(C=N)$  1644;  $\nu$ (skeletal vibration) 1596;  $\nu(SCN^-)$  2078, 2091;  $\nu(H_2O)$  3270.  $\lambda_{Max/nm}$ (solid, reflectance): 627, 1013.

### 2.2.2. Preparation of $[Ni(HL)(SCN)_2(4,4'-bipy)]$ (**2**)

Complex **2** was prepared by following a similar procedure as mentioned for the preparation of complex **1**. Here a 5 mL methanolic solution of 4,4'-bipyridine (0.156 g, 1 mmol) was added in at the end and the resulting solution was stirred again for 2 h. The final solution was filtered and kept in a  $CaCl_2$  desiccator. After 7 days, light green coloured crystals suitable for X-ray data analysis were obtained. Yield 56%. *Anal.* Calc. for  $C_{25}H_{27}N_7O_1S_2Ni$ : C, 53.15; H, 4.78; N, 17.36. Found: C, 53.19; H, 4.83; N, 17.31%. IR (KBr,  $cm^{-1}$ ):  $\nu(C=N)$  1647;  $\nu$ (skeletal vibration) 1597;  $\nu(SCN^-)$  2086.  $\lambda_{max/nm}$ (solid, reflectance): 594, 898, 1189.

*Caution! Transition metal perchlorate complexes are potentially explosive and should be handled in small amounts and with proper precautions [36].*

### 2.3. X-ray structural determination

The X-ray crystallographic data of the two compounds were collected on a Bruker-AXS SMART CCD diffractometer at 100(2) K. The crystallographic data, conditions retained for the intensity data collection and some features of the structure refinements are listed in Table 1. The intensities were collected with Mo-K $\alpha$  radiation ( $\lambda = 0.71073 \text{ \AA}$ ). Data processing, Lorentz-polarization and absorption corrections were performed using SAINT, SMART and the SADABS computer programs [37]. The structures were solved by direct methods and refined by full-matrix least-squares methods on  $F^2$ , using the SHELXTL program package [38]. All non-hydrogen atoms were refined anisotropically. The hydrogen atoms were located from difference Fourier maps, assigned with isotropic displacement factors and included in the final refinement cycles by use of HFIX (H bonded to parent C atom) or DFIX (H bonded to parent N or O atom) of the SHELXTL program. In the case of **2**, the electron density of disordered lattice water molecules was excluded by applying the SQUEEZE procedure [39]. Molecular plots were performed with the Mercury program [40].

**Table 1**

Crystallographic data and refinement parameters for complexes **1** and **2**

	<b>1</b>	<b>2</b>
Formula	C <sub>15</sub> H <sub>21</sub> N <sub>5</sub> NiO <sub>2</sub> S <sub>2</sub>	C <sub>25</sub> H <sub>27</sub> N <sub>7</sub> NiOS <sub>2</sub>
Formula Weight	426.20	564.37
Crystal System	Monoclinic	Monoclinic

Space group	P21/n (No. 14)	C2/c (No. 15)
a [Å]	7.9483(8)	37.403(2)
b [Å]	20.843(2)	9.7786(11)
c [Å]	11.0975(12)	16.1493(14)
$\alpha$ [deg]	90	90
$\beta$ [deg]	98.861(15)	106.416(14)
$\gamma$ [deg]	90	90
V [Å <sup>3</sup> ]	1816.5(3)	5665.8(10)
Z	4	8
D(calc) [g/cm <sup>3</sup> ]	1.558	1.323
Mu(MoKa) [/mm ]	1.317	0.862
F(000)	888	2352
Crystal Size [mm]	0.10 x 0.15 x 0.18	0.20 x 0.23 x 0.30
Temperature [K]	100	100
Radiation [Å]	MoK $\alpha$ 0.71073	MoK $\alpha$ 0.71073
$\Theta$ Min-Max [Deg]	2.0, 26.3	2.2, 26.4
Tot., Uniq. Data, R(int)	14262, 3690,	22062, 5789,
	0.043	0.030
Observed data [I > 2.0 $\sigma$ (I)]	3299	5344
Refinement Nref, Npar	3690, 238	5789, 333
R, wR2, S	0.0468, 0.1055,	0.0483, 0.1272,
	1.17	1.11

## 2.4. Computational details

All the initial structures were first constructed using the Spartan package [41]. Initial optimizations for the constructed structures were performed with the PM3 semi-empirical method using the Spartan package [41], then density functional theory (DFT) calculations were carried out using the GAMESS package [42,43]. Gradient corrected geometry optimizations were performed using the Steven-Basch-Karuss-Jasien-Cundari (SBKJC) [44-46] and the 6-31G basis sets. The structures were calculated by the code in GAMESS using the Tao-Perdew-Staroverov-Scuseria functional (TPSS) [47]. Vibrational harmonic frequency analyses of the optimized structures were computed to examine the minima structures with no imaginary frequencies. The optimized structures for the two complexes were compared to the crystal structures. Furthermore, intermediates along the isomerization process were predicted and optimized with the aim of understanding the mechanism of the process.

## 2.5. Bioactivity

### 2.5.1. Cell culture

HeLa (human cervical cancer cell line) and MCF-7 (human breast cancer cell line) cells were maintained in Dulbecco's modified eagle medium (DMEM), supplemented with 10% fetal bovine serum (FBS), antibiotic solution (1000 IU of penicillin and 10mg/mL streptomycin), at 37 °C in a humidified atmosphere of 5% CO<sub>2</sub>.

### 2.5.2. Cytotoxicity assay

Cell cytotoxicity was assessed by an MTT assay using the MTT reagent 3-(4,5-dimethylthiazol-2-yl)-2,5 diphenyltetrazolium-bromide dye as described by Mossman [48]. Briefly, 2×10<sup>4</sup> HeLa and MCF-7 cells were seeded in 96-well culture plates with various

concentrations of complexes **1** and **2** (stock solutions were prepared in DMSO and the final working stock solutions were prepared by diluting in culture medium; the final concentration of DMSO used in the case of the IC<sub>50</sub> value is 0.1% v/v and 0.15% v/v for complexes **2** and **1** respectively). After 24 h incubation at 37 °C and 5% CO<sub>2</sub>, 10 µL of MTT solution (5 mg/mL) were added to each well, and the samples were incubated further for 2 h at 37 °C. The purple formazan crystals formed were finally dissolved in 100 µL of DMSO. Plates were then analyzed on a microplate reader at 570 nm. At least three independent experiments were carried out in triplicate. The IC<sub>50</sub> value was determined by calculating the percentage (%) cell inhibition.

$$\% \text{inhibition} = (\text{Control abs} - \text{sample abs}) / (\text{Control abs}) \times 100$$

### 2.5.3. Reactive oxygen species (ROS) measurement

Reactive oxygen species (ROS) measurement was performed using the non-fluorescent dye 2,7-dichlorofluorescein diacetate (DCFH-DA). It diffuses into the cells and gets deacetylated by esterase to form the non-fluorescent 2,7-dichlorofluorescein (DCFH). In the presence of reactive oxygen species, DCFH reacts with ROS to form the fluorescent product DCF and which gets entrapped in the cells. In a 6-well plate,  $2 \times 10^5$  HeLa cells were grown on cover slips and allowed to adhere overnight. 234 and 352 µM of complex **1** and 142 and 177 µM of complex **2** were added for 24 h. Briefly, the cells were exposed to 10 µM DCFH-DA for 30 min at 37 °C. The cells were then mounted directly in PBS, and were subjected to fluorescence microscopy [49]. DCF induced fluorescence was detected (excitation 485 nm; emission 530 nm) and photographed using a fluorescence microscope (Nikon E800, Japan).

### 2.5.4. Apoptotic assay

Morphological alterations indicating apoptosis were examined by acridine orange (AO) and ethidium bromide (EB) staining. AO tends to permeate both live and dead cells and stains the nuclei green, whereas EB is taken up by dead cells when the membrane integrity is lost and the nucleus stains orange/red.  $2 \times 10^5$  HeLa cells were seeded on cover slips in a 6-well culture plate. Complexes **1** and **2** treated HeLa cells, as indicated above, were incubated at 37 °C and 5% CO<sub>2</sub> for 24 h. The cells were washed twice and then stained with EB (100 µg/mL) for 2.5 min and with AO (100 µg/mL) for 1 min at room temperature as modified from a previously described method [50]. The cells were once again washed with PBS, mounted and then observed under a fluorescence microscope (Nikkon E800, Japan) and photographed.

#### 2.5.5. Cell cycle analysis

Flow cytometry analysis to check the cell cycle phase distribution of HeLa cells on treatment with nickel complexes **1** and **2** was carried out after staining fixed HeLa cells with propidium iodide (PI). For this,  $4 \times 10^5$  HeLa cells were seeded in a 6-well culture plate in DMEM. After 24 h the cells were exposed to the complexes with concentrations that corresponded to the IC<sub>50</sub> value and one concentration lower than the IC<sub>50</sub> value for 24 h. After treatment, the cells were collected by trypsinization, washed with PBS and fixed overnight at -20 °C in 70% ethanol. On fixation, the cells were washed again with ice cold PBS and incubated in 500 µL propidium iodide (PI) - RNase solution [1 mg/mL PI solution, Triton X-100 (0.1% v/v) and 10 mg/mL RNase] for 30 min at 37 °C as discussed [51]. The cell cycle phase distribution was analyzed by FAC Scan using Cell Quest software (Becton Dickinson).

### 3. Results and discussion

### 3.1. Syntheses and characterization

The complex **1** was prepared by adopting the template synthesis technique by treating a methanolic solution of nickel(II) perchlorate with the Schiff-base ligand HL, formed *in situ* via condensation between salicylaldehyde and N-(2-aminoethyl)-piperazine, followed by addition of an excess of sodium thiocyanate. Complex **2** was prepared by adding 4,4'-bipyridine to the methanolic solution of complex **1**. Interestingly, no new species was observed to be generated when other neutral ligands, like imidazole, pyridine-N-oxide or 2,2'-bipyridine, were added to the methanolic solution of complex **1**. The two complexes were characterized by routine physicochemical techniques as well as by X-ray single crystal structure analyses (*vide infra*). Both complexes exhibit bands due to a C=N stretch in the range 1644-1647  $\text{cm}^{-1}$  and skeletal vibrations in the range 1596-1597  $\text{cm}^{-1}$ . Complex **1** shows strong and sharp bands at 2091 and 2078  $\text{cm}^{-1}$  due to the presence of isothiocyanato ligands, most probably in two different environments, whereas complex **2** exhibits only one very strong and sharp band at 2086  $\text{cm}^{-1}$  suggesting that both coordinated isothiocyanato ligands are in the same environment [52,53]. Complex **1** also shows a broad band at 3270  $\text{cm}^{-1}$  assigned to the O-H symmetry stretching vibrational mode of a water molecule coordinated with the metal. (Fig.S1-S2 in the Supporting Information). The ambient temperature (298 K) magnetic susceptibility measurements ( $\mu_{\text{eff}} = 3.2$  B.M for **1** and 3.3 B.M. for **2**) suggest that in both complexes Ni(II) possesses an octahedral configuration. An electronic spectral study in methanol also supports an octahedral geometry around Ni(II) in both cases (Fig. S3 in the Supporting Information) [54,55]. A solid state electronic spectral study has also been performed up to the near-IR region. Complex **1** does not show a splitting of the d-d band in the range 800-1300 nm, whereas complex **2** exhibits further splitting of the d-d band in that region (Fig. S4 in the Supporting Information). Those data

suggest that complex **1** should have a *cis*-configuration, whereas complex **2** most probably adopts a *trans*-configuration [31,53,55,56].

### 3.2. Description of the crystal structures of complexes **1** and **2**

To determine the structures of complexes **1** and **2** at the atomic level we used crystal X-ray diffraction. The molecular structures that have been obtained for complexes **1** and **2** are presented in Fig. 1. Selected bond distances and angles for complexes **1** and **2** are collected in Table 2. One can see from Figure 1 that in both of the neutral and monoclinic complexes the Ni(II) centres are octahedral, ligated by O(1), N(1) and N(2) donor atoms of the Schiff base ligand in a meridional conformation. The NiN<sub>4</sub>O<sub>2</sub> octahedron in complex **1** is completed by the N(4) and N(5) atoms of two terminal isothiocyanato groups in the *cis* position and the O(2) atom of an aqua ligand. In complex **2**, the NiN<sub>5</sub>O octahedron is completed by the N(4) and N(5) atoms of two terminal NCS groups in the *trans* position and the N(6) atom of the bipyridine ligand. The Ni-N/O bond distances in both complexes are in the range 2.014(2) to 2.313(2) Å. The N(4)-Ni(1)-N(5) bond angles of the NCS ligands are 88.28(10) and 175.56(9)° for **1** and **2**, respectively. The Ni-N-C bond angles are 141.0(2) and 154.7(2)° in complex **1**, and 153.4(2) and 163.2(2)° in complex **2**. The N-C-S bond angles are in the range 177.9(3)-179.2(3)°. In complex **1** the N(1)-C(8)-C(9)-N(2) torsion angle is -58.7(3)°, while in complex **2** it is +54.6(3)°. Finally, the “piperazine” moiety of the Schiff base has a chair conformation in both complexes. In complex **1** the Ni(1)-N(2) bond is 2.313(2) Å and it is in an axial position with respect to the chair of the “piperazine” ring, whereas in complex **2** the shorter Ni(1)-N(2) bond of 2.244(2) Å is in the equatorial position.

**Table 2**Selected bond distances (Å) and bond angles (°) for complexes **1** and **2**.

Distances	(1) (X= O(2))	(2) (X= N(6))
Ni(1)-N(1)	2.019(2)	2.014(2)
Ni(1)-O(1)	2.039(2)	2.017(2)
Ni(1)-N(4)	2.048(3)	2.096(2)
Ni(1)-N(5)	2.071(3)	2.066(2)
Ni(1)-X	2.127(2)	2.117(2)
Ni(1)-N(2)	2.313(2)	2.244(2)
O(1)-C(1)	1.329(4)	1.315(3)
N(1)-C(7)	1.283(4)	1.275(3)
N(4)-C(14)	1.167(4)	1.159(3)
C(14)-S(1)	1.643(3)	1.652(3)
N(5)-C(15)	1.167(4)	1.156(4)
C(15)-S(2)	1.649(3)	1.625(3)
Angles		
N(1)-Ni(1)-O(1)	88.95(9)	89.60(8)
N(1)-Ni(1)-N(4)	173.34(10)	88.79(9)
O(1)-Ni(1)-N(4)	89.00(9)	90.64(9)
N(1)-Ni(1)-N(5)	98.16(10)	86.77(9)
O(1)-Ni(1)-N(5)	93.25(10)	89.07(9)
N(4)-Ni(1)-N(5)	88.28(10)	175.56(9)
N(1)-Ni(1)-X	88.44(9)	176.87(9)

O(1)-Ni(1)-X	90.69(9)	92.40(8)
N(4)-Ni(1)-X	85.25(9)	93.59(9)
N(5)-Ni(1)-X	172.37(10)	90.85(9)
N(1)-Ni(1)-N(2)	81.09(9)	82.69(8)
O(1)-Ni(1)-N(2)	170.02(9)	172.28(8)
N(4)-Ni(1)-N(2)	100.98(10)	89.38(8)
N(5)-Ni(1)-N(2)	87.51(10)	90.31(9)
N(2)-Ni(1)-X	89.74(9)	95.30(8)
C(14)-N(4)-Ni(1)	154.7(2)	163.2(2)
N(4)-C(14)-S(1)	179.2(3)	179.1(2)
C(15)-N(5)-Ni(1)	141.0(2)	153.4(2)
N(5)-C(15)-S(2)	177.9(3)	178.6(3)

**Table 3**Hydrogen bonding system for complex **1** and complex **2**

D-H...A <sup>a</sup>	Symmetry of A	D...A (Å)	D-H...A (°)
<b>Compound 1</b>			
N(3)-H(90)...O(1)	[x+1/2,-y+1/2,z-1/2]	2.635(3)	169(4)
N(3)-H(91)...S(2)	[x+1,y,z]	3.434(3)	170(3)
O(2)-H(92)...S(1)	[x+1/2,-y+1/2,z+1/2]	3.184(2)	172(3)
O(2)-H(93)...S(2)	[x+1/2,-y+1/2,z+1/2]	3.384(2)	175(3)

Compound <b>2</b>			
N(3)-H(90)...S(1)	[x,-y,z-1/2]	3.290(2)	146(2)
N(3)-H(91)...N(7)	[-x,-y,-z]	2.813(3)	172(3)

Fig. 1 (a) ORTEP view of complex **1** and (b) ORTEP view of complex **2**.

In both complexes, the N(3) atom of the “piperazine” moiety does not coordinate to the Ni(II) centre, but acts as a donor for hydrogen bonds (see Table 3). In addition, the aqua ligand in complex **1** is also involved in hydrogen bonding interactions. Therefore, in the crystal structure of complex **1** the Ni complex molecules are linked by hydrogen bonding interactions between the aqua ligands and the N(3) atom of the “piperazine”. In complex **2** the pyridine rings of the bipyridine ligand form an interplanar angle of 24.3° and thus form polymeric layers. Fig. S5 (see Supporting Information) demonstrates the packing of the 3D polymeric chains in complexes **1** and **2**.

### 3.3. Conductometric and IR titration study

In order to visualize the change in orientation of the two coordinated isothiocyanato ligands and thereby the reaction pathway associated with the transformation of **1** to **2**, we have resorted to conductometric and solution phase FTIR spectral studies. First of all the molar conductance of **1** in a methanolic solution has been determined as  $52 \Omega^{-1} \text{cm}^2 \text{mol}^{-1}$ , indicating its non-electrolytic nature. Then a methanolic solution of 4,4'-bipyridine was added to the solution of **1** with constant slow stirring and the change in molar conductance value was monitored with time. The conductance value was observed to increase and attained a maximum value of 92

$\Omega^{-1} \text{ cm}^2 \text{ mol}^{-1}$  after 30 min of mixing. Then gradually it decreased in value and attained a constant value of  $26 \Omega^{-1} \text{ cm}^2 \text{ mol}^{-1}$  after 2 h (Fig. S6, Supporting Information). The data clearly hints that initially after addition of 4,4'-bipyridine, one thiocyanato ligand undergoes dissociation and giving a 1:1 electrolyte, then after 2 h the dissociated SCN again ligates to produce **2**, which is a non-electrolyte.

Fig. 2(a) depicts the solid state overlapped FT-IR spectra of **1** and **2** in the range 1900-2250  $\text{cm}^{-1}$ , the fingerprint region for the SCN stretching frequency. In **1** the SCN groups are in the *cis* position, whereas in **2** they have a *trans* orientation. A solution phase ATR study has been carried out according to the following manner. First, the FT-IR spectrum of **1** in methanol was recorded [Fig. 2 (b)(i)], which shows two bands centered at 2107 and 2010  $\text{cm}^{-1}$ , characteristic of *cis*-thiocyanato groups. Then 4,4'-bipyridine was added to the solution of **1** with stirring and spectra were recorded after 30 min [Fig. 2 (b)(ii)], 1 h [Fig. 2 (b)(iii)] and 2 h [Fig. 2 (b)(iv)]. It is very clear from those spectra that after 2 h the complete transformation of the coordinated isothiocyanato ligands from the *cis* to *trans* orientation takes place, as is evident from the generation of a new band at 2045  $\text{cm}^{-1}$ , with the earlier two bands completely vanishing.

We have also performed an experiment where complex **2** is treated with excess water, with the view to understand whether complex **1** could be regenerated from complex **2** on dilution. We did not get any change in the FT-IR spectral pattern on dilution and thereby nullify that possibility. This fact also implies that complex **2** is more stable than **1** and that view has further been supported by DFT calculations (*vide infra*).

Fig.2 (a) Overlapped FT-IR spectra of complexes **1** and **2** in the range 1900-2250  $\text{cm}^{-1}$  in the solid state. (b) FT-IR spectra of the transformation of the *cis* to *trans* arrangement of the

isothiocyanate ligands in solution (i) before addition of 4,4'-bipyridine; (ii) 30 min after addition of 4,4'-bipyridine; (iii) 1 h after addition of 4,4'-bipyridine and (iv) 2 h after addition of 4,4'-bipyridine.

### 3.4. Geometry optimization and computed IR spectra of complexes **1** and **2**

The *cis*-orientation of the two isothiocyanato ligands in complex **1** changes into a *trans* one after addition of 4,4'-bipyridine. To rationalize the fact via DFT calculations, first we optimized complexes **1** and **2** (see Fig. 3). The optimized results suggest that **2** is more stable than **1** by almost 43 kcal/mol. To get a more clear picture we optimized an analogous molecule to complex **2**, but where the two SCN<sup>-</sup> ligands are in a *cis* fashion and the bipyridine ligand is in an axial position, namely *cis*-[Ni(HL)(NCS)<sub>2</sub>(4,4'-bipyridine)] (see Fig. S7 in the Supporting Information). This hypothetical molecule has ~60 kcal/mol higher energy than complex **2**. Thus, the energy calculations clearly hints why complex **2** is formed from **1** on addition of 4,4'-bipyridine instead of *cis*-[Ni(HL)(NCS)<sub>2</sub>(4,4'-bipyridine)].

Fig. 3 Optimized geometries of complexes **1** and **2**.

To examine the minima of the complexes, the vibrational frequencies were computed and they showed no imaginary frequencies. We have summarized the computed bonds and angles to illustrate the comparison between the computed values and experimental values for complexes **1** and **2** (see Table S1-S2 in Supporting Information). From these tables it is evident that the computed values are in good agreement with the experimental results. The averaged deviations

for the distances in complexes **1** and **2** are ~ 4% and ~ 5% and for the angles they are ~ 4 % and ~ 15%, respectively.

We further compared the calculated vibrational frequencies to the experimental vibrational frequencies. Tables 4 and 5 summarize the selected vibrational frequencies of complexes **1** and **2**, respectively. Here also the calculated vibrational frequencies are in excellent agreement with the observed vibrational frequencies.

**Table 4**

Selected vibrational frequencies of complex **1**.

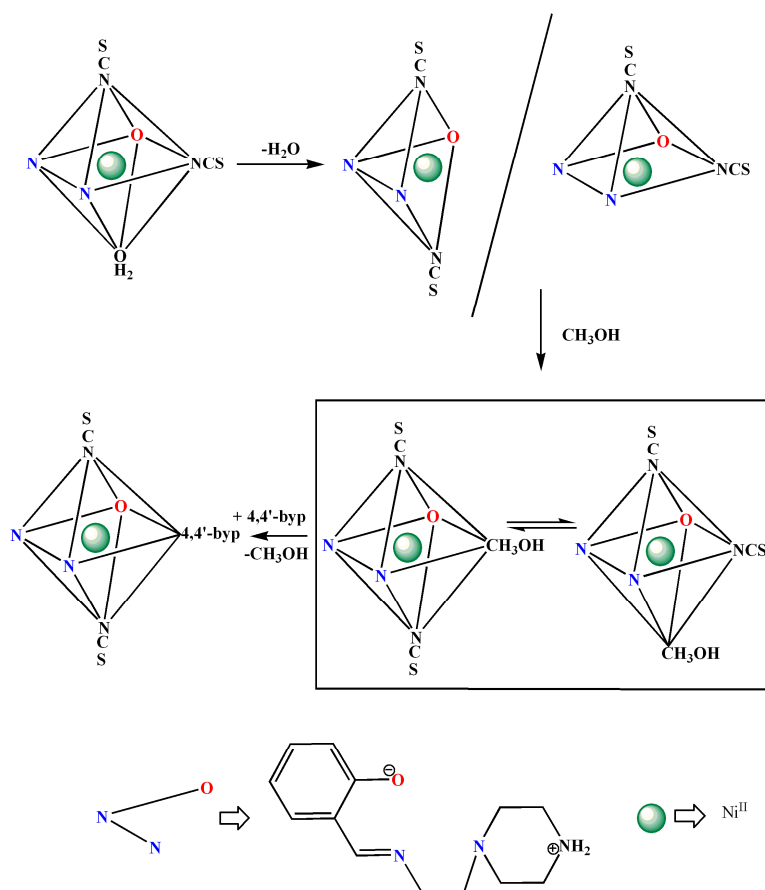
Vibrational mode description	Calc. frequency ( $\text{cm}^{-1}$ )	Exp. frequency ( $\text{cm}^{-1}$ )
Benzene ring mode	1590	1596
Stretching of C=N	1639	1644
Stretching of SCN	1998	2016
	2130	2107
H <sub>2</sub> O	3283	3270

**Table 5**

Selected vibrational frequencies of complex **2**.

Vibrational mode description	Calc. frequency ( $\text{cm}^{-1}$ )	Exp. frequency ( $\text{cm}^{-1}$ )
Benzene ring mode	1536	1597
Stretching of C=N	1636	1647

From the results of the conductometric and FTIR titrations we proposed a probable mechanistic pathway of the observed interesting transformation (Scheme 2) and tried to correlate them using energy minimization. To understand the mechanism of the formation of *trans*-[Ni(HL)(NCS)<sub>2</sub>(4,4'-bipyridine)] from *cis*-[Ni(HL)(SCN)<sub>2</sub>(H<sub>2</sub>O)] we predicted more than ten optional intermediates (not all shown here), considering the various ligands that might replace the aqua ligand and the two NCS<sup>-</sup> ligands of the complexes. Our calculations predicted three intermediates along the transformation process. It should be noted here that we did not calculate the activation energies, the transition states or the barriers. Here, we present only the energy differences between the intermediates along the proposed mechanistic pathway. Fig. 4 illustrates the energy associated with the complexes and the probable intermediates in the proposed mechanism.



Scheme. 2 Probable mechanism of the formation of *trans*-[Ni(HL)(NCS)<sub>2</sub>(4,4'-bipyridine)] from *cis*-[Ni(HL)(SCN)<sub>2</sub>(H<sub>2</sub>O)].

Fig. 4 Energy profile diagram of the formation of complex **2** from complex **1**.

Our calculations suggest that in the first step the aqua ligand “leaves” the Ni(II) centre from complex **1** to form intermediate I, which has *trans* located SCN groups. This process is endothermic and probably occurs when complex **1** is solvated in methanol. The *cis* orientation of the two SCN groups is less preferred, since the *cis* complex without the aqua ligand showed an energetically less stable structure (by ~ 12 kcal/mol). In the next step methanol “replaces” the aqua ligand to form a *cis* or *trans* complex, i.e., intermediates II or III. The energy difference

between these two intermediates is  $\sim 0.31$  kcal/mol (with the *cis* complex being slightly more stable than the *trans* complex), thus we suggest that an equilibrium between these two intermediates occurs in this step. This step, which is exothermic, is likely to be very crucial in the transformation process, since it determines whether the bipyridine ligand will lead to the *cis* complex or the *trans* complex. As noted above, the *trans* complex is energetically more stable than the *cis* complex by 60 kcal/mol, thus after adding bipyridine to the solution, *trans*-[Ni(HL)(NCS)<sub>2</sub>(4,4'-bipyridine)] is formed.

We also computed the IR spectra of these three intermediates by following the  $\nu_{\text{SCN}}$  vibrational frequency. Intermediate I exhibited two vibrational frequencies at 2120 and 2036  $\text{cm}^{-1}$ , intermediates II and III also showed two vibrational frequencies: Intermediate II at 2135 and 2008  $\text{cm}^{-1}$  and intermediate III at 2117 and 1999  $\text{cm}^{-1}$ . However, the final product *trans*-[Ni(HL)(NCS)<sub>2</sub>(4,4'-bipyridine)] revealed only one vibrational frequency at 2044  $\text{cm}^{-1}$ . In summary, bipyridine plays role in stabilizing the complex and in forming a complex that is characterized by only one band for  $\nu_{\text{SCN}}$  in the IR spectrum.

### 3.5. Bio-activity study

#### 3.5.1. Cytotoxicity assay

The cytotoxic potential of complexes **1** and **2** was tested on HeLa and MCF-7 cells. Treatment of HeLa and MCF-7 cells with the complexes for 24 h resulted in growth inhibition (Fig. 5). Complex **2** showed a cytotoxic effect at  $\text{IC}_{50} = 177 \mu\text{M}$  (100  $\mu\text{g}/\text{mL}$ ), while complex **1** showed cytotoxic activity at  $\text{IC}_{50} = 351 \mu\text{M}$  (150  $\mu\text{g}/\text{mL}$ ) for HeLa cells. At the same time both complexes showed quite a low cytotoxic effect on MCF-7 cells, with  $\text{IC}_{50}$  values around 410  $\mu\text{M}$  (175  $\mu\text{g}/\text{mL}$ ) for complex **1** and 355  $\mu\text{M}$  (200  $\mu\text{g}/\text{mL}$ ) for complex **2**. The percentage of cell

inhibition with respect to complexes **1** and **2** against both the cell lines are shown in Fig. 5A and 5B. Our results indicate that complex **2** is more efficient in inhibiting the growth of HeLa cells in comparison to complex **1** after 24 h. However, in the case of MCF-7 cells, both complexes exhibited a low cytotoxic activity as compared to HeLa cells. It is important to note that the concentration of DMSO is so low that it will not show any toxicity, as the cytotoxicity of DMSO is more than 1% in the case of normal cells. In 2013, a study by Milenkovi *et al* also showed the cytotoxic activity of three square-planar complexes of Ni(II) with ethyl (2E)-2-[2 (diphenylphosphino)benzylidene]hydrazinecarboxylate and monodentate pseudohalides, the appropriate ligand, and a nickel salt by MTT assay after 48 h treatment in six tumor cell lines (A549, MDA-MB-361, HeLa, FemX, LS-174 and K562) [57]. They reported that all the complexes showed cytotoxicity towards all cell lines and the activity was increased compared to the ligand and also the complexes showed more cytotoxicity towards K562 cells in comparison to other cell lines. Similarly, the antiproliferative activities of three complexes, Mn(II), Ni(II) and Cu(II), of demethylcantharate and 2-aminopyridine and [Na<sub>2</sub>(DCA)] against human hepatoma cells (SMMC- 7721) and human gastric cancer cells (MGC80-3) also showed that the complexes had a strong antiproliferative effect against the two types of cancer cells [58].

Fig. 5 The cytotoxicity profile of Ni complexes **1** and **2** against HeLa [A] and MCF-7 [B] cells at different concentrations was estimated by an MTT assay. Data are expressed as a percentage of control  $\pm$  SEM from three independent experiments.

### 3.5.2. ROS measurement

Based on the results obtained from the cell cytotoxicity assay, we found that the nickel(II) complexes showed more activity towards HeLa than MCF-7 cells, therefore the HeLa cell line was selected for further investigations related to anticancer activity. To examine the generation of ROS in HeLa cells on treatment with the complexes, DCFH-DA dye was used. HeLa cells were exposed to DCFH-DA after treatment with complexes **1** and **2**, along with a control, for 24 h. Both the complexes induced ROS generation in a concentration dependent manner after 24 h, as reflected by the increase in fluorescence intensity (Fig. 6). A higher amount of ROS was generated at their IC<sub>50</sub> values [complex **1** - 150 µg/mL (351 µM) and complex **2** - 100 µg/mL (177 µM)] than at a concentration lower than the IC<sub>50</sub> value in comparison to the control (Fig. 6). ROS is found to trigger apoptosis in cells [59]. Some other nickel and copper derivatives [Ni(II) and Cu(II) N(4)-ethylmorpholine citronellal thiosemicarbazone] also triggered ROS generation in the HT29 cell line, showing a remarkable and rapid ROS increase, and it was proposed that perhaps the ROS could be mediating the process of cellular damage [60]. Similarly, changes in the intracellular ROS were detected using fluorescence spectrometry and the fluorescence intensity was measured by DCF after treatment of HeLa cells for 6 h with the Cu(II) complex of the ethyl 2-[bis (2-pyridylmethyl) amino] propionate ligand and the results showed that the concentration of the ROS increased in a dose- and time-dependent manner compared to a control group [61].

On the basis of our results, we suggest that both the Ni complexes could induce apoptosis in cancer cells, as a ROS is generated which may lead to cellular damage. To validate the above statement, we performed fluorescent staining with acridine orange and ethidium bromide to analyse the apoptosis.

Fig. 6 Detection of a ROS by measuring the fluorescence intensity in HeLa cells using a DCFH-DA probe under a fluorescence microscope. Cells were treated with 234 and 351  $\mu\text{M}$  of complex **1** and 142 and 177  $\mu\text{M}$  of complex **2** for 24 h.

### 3.5.3. Apoptotic assay

During apoptosis various structural changes take place, like nuclear and cytoplasmic condensation, breaking up of the cell into membrane bound fragments and formation of apoptotic bodies which are engulfed and undergo autolysis within phagosomes, and are rapidly degraded by lysosomal enzymes [62]. The AO/EB staining of HeLa cells was done to determine apoptosis on treatment with complexes **1** and **2** (Fig. 7) and the image obtained shows the presence of apoptotic cells. The cells with green fluorescence and an intact green nucleus represent the live cells. The apoptotic morphology of cells in the treated samples shows cellular shrinkage, membrane blebbing, nuclear fragmentation and chromatin condensation. At 24 h of incubation of HeLa cells with both complexes, we observed that at a lower concentration they showed an early stage of apoptosis with presence of membrane blebbing and some cells with nuclear fragmentation, but at higher concentration, that is the  $\text{IC}_{50}$  concentration, they showed later stages of apoptosis with most of the cells undergoing nuclear fragmentation (Fig. 7). Similar results were also reported by Luying Li, et al in 2013, to identify the possible involvement of apoptosis in HeLa cells treated with the Cu(II) complexes CuPDTP, CuADTP and CuBFDTP for 24 h, on staining with AO and EB. Fluorescence images of the AO/EB-stained HeLa cell showed apoptotic cells as well as some of them even showing secondary necrosis. On treatment of the cells with significant amounts of the Cu(II) complexes, the cells exhibited condensed orange

nuclei, which is a hallmark of late apoptotic cells; however, the necrotic cells displayed structurally intact nuclei with orange staining [63].

We therefore suggest that the results obtained in our case substantiate that the complexes induce apoptotic cell death in cancer cells that might be triggered by the process of ROS generation by the complexes.

Fig. 7 (A-E) showing AO/EB dual staining of HeLa cells to identify changes in the nuclear morphology. Figure (A) represent control cells with green fluorescence, figures (B - C) and (D - E) represent complexes **1** and **2** treated cells respectively. The blue arrows show live cells, red arrows show apoptotic cells and red dotted arrows represent the apoptotic cells with membrane blebbing.

#### 3.5.4. Cell cycle analysis

To identify whether the complexes have any effect on cell cycle phase distribution or not, cell cycle analysis was done by flow cytometry after exposure of HeLa cells to complexes **1** and **2** for 24 h. The results of the FACS analysis have been presented in the form of a histogram (Figure 8) which shows that both the complexes induced a shift of cell population in the cell cycle phases compared to the control. Treatment at the  $IC_{50}$  value for both complexes **1** (351  $\mu$ M) and **2** (177  $\mu$ M) showed a pronounced effect on the cell cycle, as it induced an increase of the percentage of the cells in the S phase, but a decrease in the percentage of cells at the G1 and G2 phase, in comparison to the control, suggesting an arrest of the cell cycle in the S phase. In the case of complex **1** about 15% of cells are in the S phase at its  $IC_{50}$  value, and in the case of complex **2** double the number of cells, that is 18%, are in the S phase at its  $IC_{50}$  value, as

compared to the control. In the same manner, Milenkovi *et al.* in 2013 also reported three square-planar complexes of Ni(II) with ethyl (2E)-2-[2-(diphenylphosphino) benzylidene] hydrazinecarboxylate and monodentate pseudohalides that caused changes in the cell cycle distribution. They showed that all the investigated nickel complexes induced an increase of the percentage of cells in the sub-G1 phase and a decrease of the percentage of cells in the G1 phase compared to the control, while two of their compounds induced an increase in the percentage of cells in the S and G2 phase only at the highest concentration [57].

Fig. 8 Analysis of the cell cycle distribution of HeLa cells on treatment with complexes **1** and **2** after 24 h by flow cytometry analysis. Control (a), and after 24 h treatment with nickel complexes **1** (b-c) and **2** (d-e).

### 3.6. Solid state thermal studies of complexes **1** and **2**

The thermal stabilities of complexes **1** and **2** have been investigated using thermogravimetric analysis (TGA) in the temperature range 30-700 °C in a single run in a dynamic nitrogen environment. The TGA results for complexes **1** and **2** are shown in S8 (see Supporting Information). The TGA results for complexes **1** and **2** indicate that the complexes are stable up to 80 and 136 °C, respectively. For complex **1**, the first step weight loss is 4.5% (calc. 4.88%) in the temperature range 80-160 °C, which corresponds to the loss of one coordinated water molecule. In the IR spectrum, the broad band at around 3270 cm<sup>-1</sup> that was observed for complex **1** is due to an OH stretching vibration, and this band was absent in the dehydrated species, confirming the elimination of the water molecule on heating. For complex **2**, the weight loss starts at 136 °C. One can see that in the case of complex **2**, two steps of decomposition occur:

one appears at 136 °C and second after heating over 136 °C. Finally, for both complexes **1** and **2**, NiO is obtained as the thermally stable final product, which is further characterised by PXRD (see S9 in Supporting Information file). For complex **1** the total experimental weight loss is 82.37% (calc. 82.6%) at 609 °C and for complex **2** the total experimental weight loss is 87.3% (calc. 86.7%) at 559 °C.

#### 4. Conclusions

On reaction of the Schiff base ligand 2-[(2-piperazin-1-yl-ethylimono)-methyl]phenol (HL), prepared via condensation of salicylaldehyde and N-(2-aminoethyl)-piperazine, with nickel(II) perchlorate followed by sodium thiocyanate, complex **1**, [Ni(HL)(SCN)<sub>2</sub>(H<sub>2</sub>O)] is obtained. X-ray single crystal structural analysis reveals that the nitrogen atom of the piperazine moiety is protonated, which is responsible for the coordination of two isothiocyanato ligands to attain electroneutrality and the two isothiocyanato ligands are in the *cis* position. Complex **1** on reaction with 4,4'-bipyridine (4,4'-bpy) yields another mononuclear complex, [Ni(HL)(SCN)<sub>2</sub>(4,4'-bpy)] (**2**), with the configuration of the isothiocyanato ligands changing from *cis* to *trans*. This configuration change has been monitored by IR titration and conductometric studies, and a reaction mechanism has been proposed. Detailed DFT calculations, which reveal the higher stability of the *trans* species by ~43 kcal mol<sup>-1</sup> over the *cis* one, have been performed to rationalize the proposed mechanism. The bioactivity of the two well characterized complexes as antitumor agents has been investigated extensively. The synthesized nickel complexes show good anticancer activity. Both the complexes exhibited cytotoxicity towards the tested cancer cell lines, having a preference to the HeLa cell line over the MCF-7 cell line. The activity of both complexes was shown from the cell cycle distribution (increase of

the percentage of cells in the S-phase and decrease of the percentage of cells in the G1 phase) and the property to induce generation of ROS, possibly leading to apoptotic cell death. Both the complexes are found to be active, though complex **2** seems to be more promising. Further detailed investigation, which is underway in our laboratory, is necessary to find out the applicability of the *trans*-variety as an antitumor agent and to find out the reason, most likely different from the operative mechanism of *cis*-platin, behind the better activity of the *trans* species.

#### **Appendix A. Supplementary data**

CCDC 971172 and 971173 contain the supplementary crystallographic data for complexes **1** and **2**. These data can be obtained free of charge via <http://www.ccdc.cam.ac.uk/conts/retrieving.html>, or from the Cambridge Crystallographic Data Centre, 12 Union Road, Cambridge CB2 1EZ, UK; fax: (+44) 1223-336-033; or e-mail: [deposit@ccdc.cam.ac.uk](mailto:deposit@ccdc.cam.ac.uk). Supplementary data associated with this article can be found in the online version.

#### **Acknowledgements**

This work was supported by the Council of Industrial and Scientific Research, New Delhi [CSIR project no. 01(2464)/11/EMR-II dated 16-05-2011 to DD]. The authors wish to thank the Head, Department of Zoology, Faculty of Science, Banaras Hindu University for extending laboratory facilities and the Coordinator, Interdisciplinary school of life sciences, Banaras Hindu University for providing the FACS facility.

#### **References**

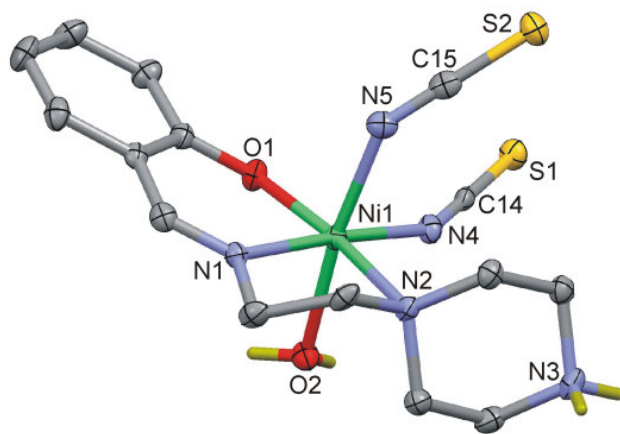
- [1] R. Prabhakaran, P. Kalaivani, P. Poornima, F. Dallemer, G. Paramaguru, V. Vijaya Padma, R. Renganathan, R. Huang, K. Natarajan, Dalton Trans. 41 (2012) 9323.
- [2] T.M. Hunter, L.W. McNae, D.P. Simpson, A.M. Smith, St. Moggach, F. White, M.D. Walkinshaw, S. Parsons, P.J. Sadler, Chem.Eur. J. 13 (2007) 40.
- [3] X. Dong, X. Wang, Y. He, Z. Yu, M. Lin, C. Zhang, J. Wang, Y. Song, Y. Zhang, Z. Liu, Yi. Li, Z. Guo, Chem. Eur. J. 16 (2010) 14181.
- [4] M. Ethirajan, P. Chen, T.Y. Ohulchanskyy, L.N. Goswami, A. Gupta, A. Srivatsan, M.P. Dobhal, J.R. Missert, P.N. Prasad, K.M. Kadish, R.K. Pandey, Chem. Eur. J. 19 (2013) 6670.
- [5] D-M. Kong, J. Wang, L-N. Zhu, Y-W. Jin, X-Z. Li, H-X. Shen, H-F Mi, J. Inorg. Biochem. 102 (2008) 824.
- [6] L-N. Zhu, D-M. Kong, X-Z. Li, G-Y. Wang, J. Wang, Y-W. Jin, Polyhedron 29 (2010) 574.
- [7] F. Le, D. Sun, D. Liu, C. Zheng, Y. Liu, J. Liu, Inorg. Chem. Comm. 38 (2013) 20.
- [8] K.C. Skyrianou, F. Perdih, A.N. Papadopoulos, I. Turel, D.P. Kessissoglou, G. Psomas, J. Inorg. Biochem. 105 (2011) 1273.
- [9] N. Selvakumaran, N.S.P. Bhuvanesh, A. Endo, R. Karvembu, Polyhedron 75 (2014) 95.
- [10] E. Ferentinos, D. Maganas, C.P. Raptopoulou, A. Terzis, V. Psycharis, N. Robertson, P. Kyritsis, Dalton Trans. 40 (2011) 169.
- [11] D. Maganas, A. Grigoropoulos, S.S. Staniland, S.D. Chatziefthimiou, A. Harrison, N. Robertson, P. Kyritsis, F. Neese, Inorg. Chem. 49 (2010) 5079.
- [12] J. Li, H. Song, C. Cui, J-P. Cheng, Inorg. Chem. 47 (2008) 3468.

- [13] O. Rotthaus, F. Thomas, O. Jarjayes, C.P.E. Saint-Aman, J-L. Pierre, *Eur. J. Inorg. Chem.* 12 (2006) 6953.
- [14] S. Mukhopadhyay, D. Mandal, D. Ghosh, I. Goldberg, M. Chaudhury, *Inorg. Chem.* 42 (2003) 8439.
- [15] S. Blanchard, F. Neese, E. Bothe, E. Bill, T. Weyhermüller, K. Wieghardt, *Inorg. Chem.* 44 (2005) 3636.
- [16] R. Carrasco, J. Cano, X. Ottenwaelder, A. Aukauloo, Y. Journaux, R. Ruiz-Garcia, *Dalton Trans.* (2005) 2527.
- [17] J. Adhikary, P. Chakraborty, S. Das, T. Chattopadhyay, A. Bauzá, S.K. Chattopadhyay, B. Ghosh, F.A. Mautner, A. Frontera, D. Das, *Inorg. Chem.* 52 (2013) 13442.
- [18] S. Tobich, *Acc. Chem. Res.* 35 (2002) 96.
- [19] C-Y. Liao, K-T. Chan, Y-C. Chang, C-Y. Chen, C-Y. Tu, C-H. Hu, H. M. Lee, *Organometallics* 26 (2007) 5826.
- [20] M. I. Lipschutz, X. Yang, R. Chatterjee, T.D. Tilley, *J. Am. Chem. Soc.* 135 (2013) 15298.
- [21] Z. Xu, L.K. Thompson, V.A. Milway, L. Zhao, T. Kelly, D.O. Miller, *Inorg. Chem.* 42 (2003) 2950.
- [22] P. Mukherjee, C. Biswas, M.G.B. Drew, A. Ghosh, *Polyhedron* 26 (2007) 3121.
- [23] R. Jothibas, K-W. Huang, H.V. Huynh, *Organometallics* 29 (2010) 3746.
- [24] D. Das, A. Ghosh, N. R. Chaudhuri, *Thermochim. Acta.* 287 (1996) 155.
- [25] R. Laskar, D. Das, G. Mostafa, A.J. Welch, N.R. Chaudhuri, *Acta Chem. Scand.* 52 (1998) 702.
- [26] S. L. Moore, P.J. Squattrito, *Acta Crystallogr., Sect. C.* 55 (1999) 332.

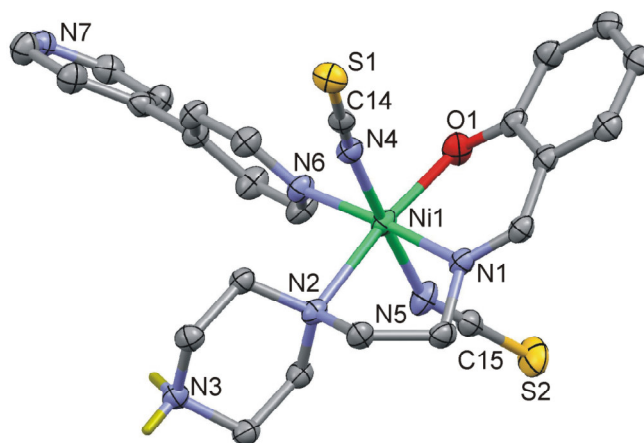
- [27] M. James, H. Kawaguchi, K. Tatsumi, *Polyhedron* 17 (1998) 1571.
- [28] A.K. Mukherjee, M. Mukherjee, S. Ray, A. Ghosh, N.R. Chaudhuri, *J. Chem. Soc., Dalton Trans.* (1990) 2347.
- [29] S. Ghosh, M. Mukherjee, A.K. Mukherjee, N.R. Chaudhuri, *Acta Crystallogr.* 53 (1997) 1561.
- [30] I.R. Laskar, T.K. Maji, S. Chaudhuri, A. Ghosh, N.R. Chaudhuri, *Polyhedron* 19 (2000) 1803.
- [31] M. Ghosh, A. Majee, M. Nethaji, T. Chattopadhyay, *Inorg. Chim. Acta.* 362 (2009) 2052.
- [32] C. Pariya, A. Ghosh, N.R. Chaudhuri, S. Ghosh, M. Mukherjee, A.K. Mukherjee, *Polyhedron* 15 (1996) 1643.
- [33] S. Chattopadhyay, P. Chakraborty, M.G.B. Drew, A. Ghosh, *Inorg. Chim. Acta.* 362 (2009) 502.
- [34] S. Mondal, T. Chattopadhyay, S.K. Neogi, T. Ghosh, A. Banerjee, D. Das, *Mater. Lett.* 65 (2011) 783. (b) G.N. Giovana, A.S. Gulaim, G.K. Vadim, *Cryst. Growth Des.* 11 (2011) 1238. (c) T. Ghosh, T. Chattopadhyay, S. Das, S. Mondal, E. Suresh, E. Zangrando, D. Das, *Cryst. Growth Des.* 11 (2011) 3198.
- [35] T. Ghosh, S.K. Dash, P. Chakraborty, A. Guha, K. Kawaguchi, S. Roy, T. Chattopadhyay, Debasis Das, *RSC Adv.* 4 (2014) 15022.
- [36] W.C. Wolsey, *J. Chem. Educ.*, 50 (1973) A335.
- [37] (a) Bruker (2005) SAINT v. 7.23; Bruker (2006) SMART; Bruker AXS Inc. Madison, Wisconsin, USA; (b) G.M. Sheldrick (2001), SADABS v. 2. University of Gottingen, Germany.
- [38] G.M. Sheldrick, *Acta Crystallogr.* A64 (2008) 112.

- [39] A.L. Spek, *J. Appl. Crystallogr.* 36 (2003) 7.
- [40] C.F. Macrae, I.J. Bruno, J.A. Chisholm, P.R. Edgington, P. McCabe, E. Pidcock, L. Rodriguez-Monge, R. Taylor, J. van de Streek, P.A. Wood, *J. Appl. Crystallogr.* 41 (2008) 466.
- [41] <http://www.wavefun.com/products/spartan.html>.
- [42] M.W. Schmidt, K.K. Baldrige, J.A. Boatz, S.T. Elbert, M.S. Gordon, J.H. Jensen, S. Koseki, N. Matsunaga, K.A. Nguyen, S.J. Su, T.L. Windus, M.J.A. Dupuis, Montgomery, General Atomic and Molecular Electronic-Structure System. *J. Comput. Chem.* 14 (1993) 1347.
- [43] <http://www.msg.ameslab.gov/GAMESS/GAMESS.html>.
- [44] W.J. Stevens, H. Basch, M. Krauss, *J. Chem Phys.* 81 (1984) 6026.
- [45] W.J. Stevens, M. Krauss, H. Basch, P.G. Jasien, *Can. J. Chem.* 70 (1992) 612.
- [46] T.R. Cundari, W.J. Stevens, *J. Chem. Phys.* 98 (1993) 5555.
- [47] J.P. Perdew, J.M. Tao, V.N. Staroverov, G.E. Scuseria, *J. Chem. Phys.* 120 (2004) 6898.
- [48] T. Mosmann, *J. Immunological Methods.* 65 (1983) 55.
- [49] M. Karlsson, T. Kurz, U.T. Brunk, S.E. Nilsson, C.I. Frennesson, *Biochem. J.* 428 (2010) 183.
- [50] J. Anter, Z.F. Bedmar, M.V. Pulido, S.D. Peyras, M.M. Millan, A.A. Moraga, A.M. Serrano, M.L.D. Castro, *Mutation Research* 723 (2011) 165.
- [51] J.T. Lim, G.A. Piazza, E.K. Han, T.M. Li, H. Delohery, T.S. Finn, R. Buttyan, H. Yamamoto, G.J. Sperl, K. Brendel, P.H. Gross, R. Pamukcu, I.B. Weinstein, *Biochem. Pharmacol.* 58 (1999) 1097.

- [52] T. Ghosh, J. Adhikary, P. Chakraborty, P.K. Sukul, M.S. Jana, T.K. Mondal, E. Zangrando, D. Das, Dalton Trans. 43 (2014) 841.
- [53] D. Zhu, Y. Xu, Z. Yu, Z. Guo, H. Sang, T. Liu, X. You, Chem. Mater. 14 (2002) 838.
- [54] Lever, A.B.P. Inorganic Electronic Spectroscopy, 2nd ed.; Elsevier Science Publishers BV: Amsterdam, The Netherlands, 1984; p 553.
- [55] R.M. Buchanan, M.S. Mashuta, K.J. Oberhausen, J.F. Richardson, J. Am. Chem. Soc. 111 (1989) 4497.
- [56] Y. Ihara, Y. Satake, M. Suzuki, A. Uehara, Bull. Chem. Soc. Jpn. 64 (1991) 3647.
- [57] M. Milenkovi, A. Bacchi, G. Cantoni, J. Vilipi, D. Sladi, M. Vuj, N. Gligorijevi, K. Jovanovi, S. Radulovi, K. Andelkovi, Eur. J. Med. Chem. 68 (2013) 111.
- [58] Z.F. Fan, Q.Y. Lin, X.L. Zheng, L.L. Zhang, Q. Yang, J.Y. Gu, J Fluoresc. 22 (2012) 1395.
- [59] M.B. Azad, Y. Chen, S.B. Gibson, Antioxid. Redox Signal 4 (2009) 777.
- [60] F. Bisceglie, R. Alinovi, S. Pinelli, M. Goldoni, A. Buschini, S. Franzoni, A. Mutti, P. Tarasconi, G. Pelosi, Metallomics 11 (2013) 1510.
- [61] W.J. Guo, S.S. Ye, N. Cao, J. Huang, J. Gao, Q.Y. Chen, Exp. Toxicol. Pathol. 62 (2010) 577.
- [62] J.F.R. Kerr, A.H. Wyllie, A.R. Currie, Br. J. Cancer 26 (1972) 239.
- [63] L. Li, K. Du, Y. Wang, H. Jia, X. Hou, H. Chao, L. Ji, Dalton Trans. 42 (2013) 11576.



(a)



(b)

Fig. 1.

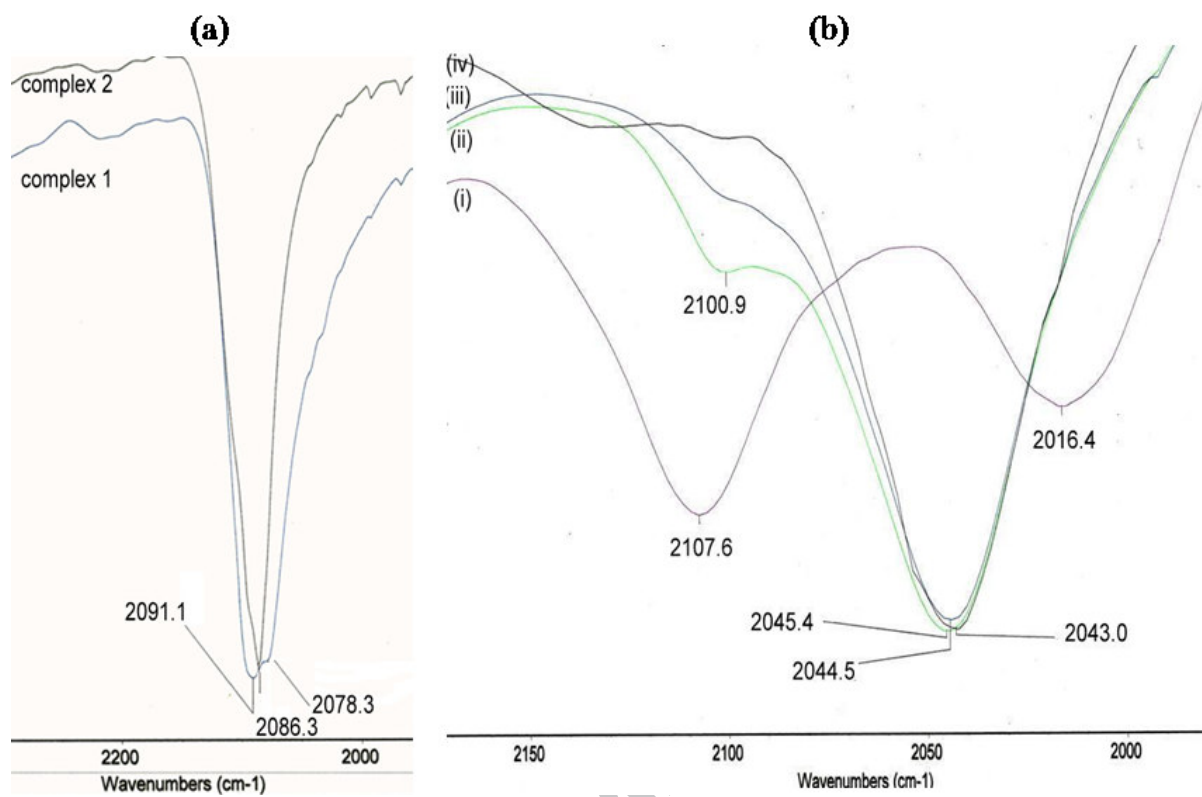


Fig.2.

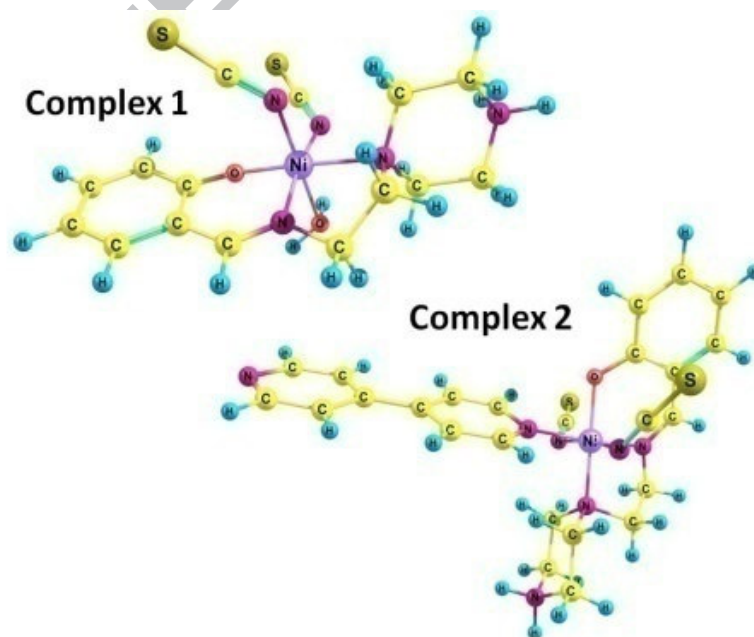


Fig. 3.

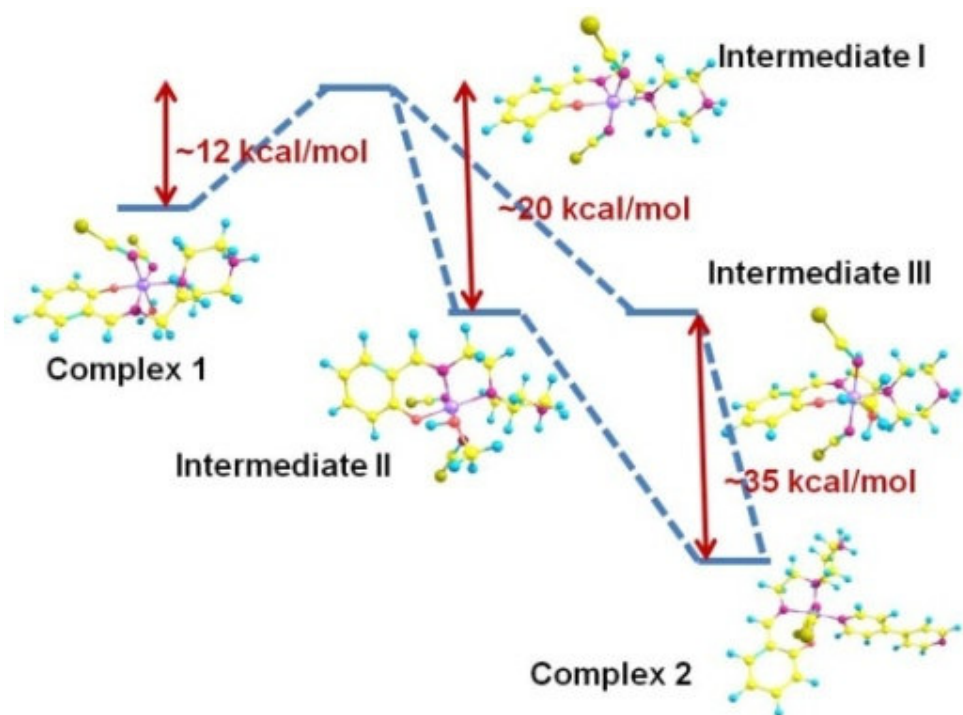


Fig. 4.

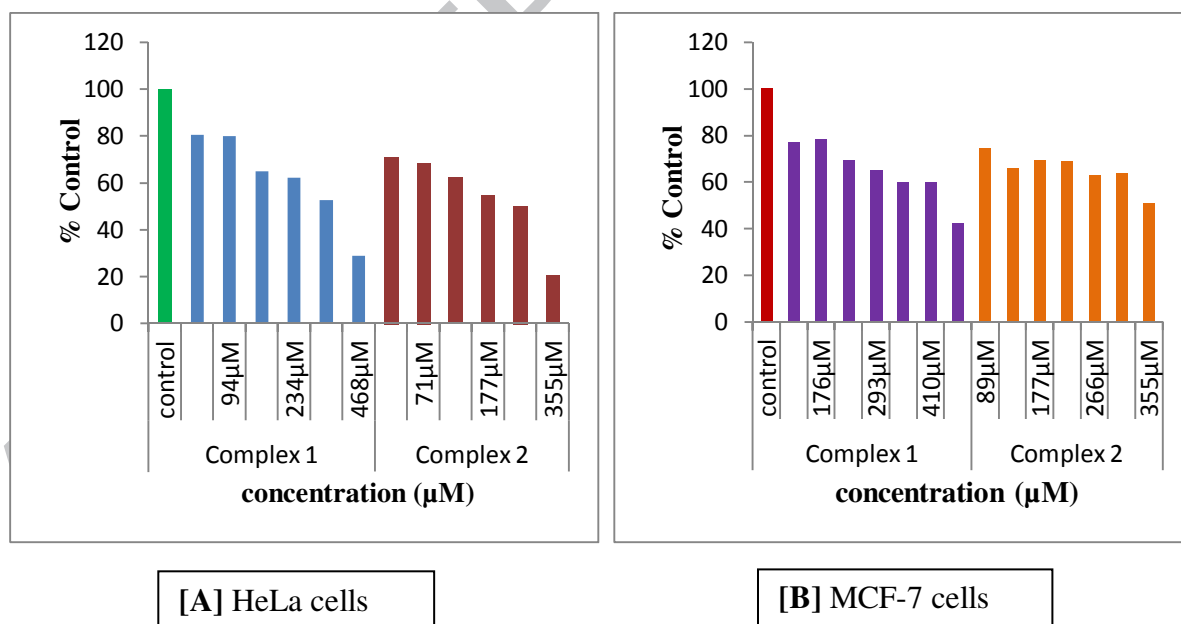


Fig. 5.

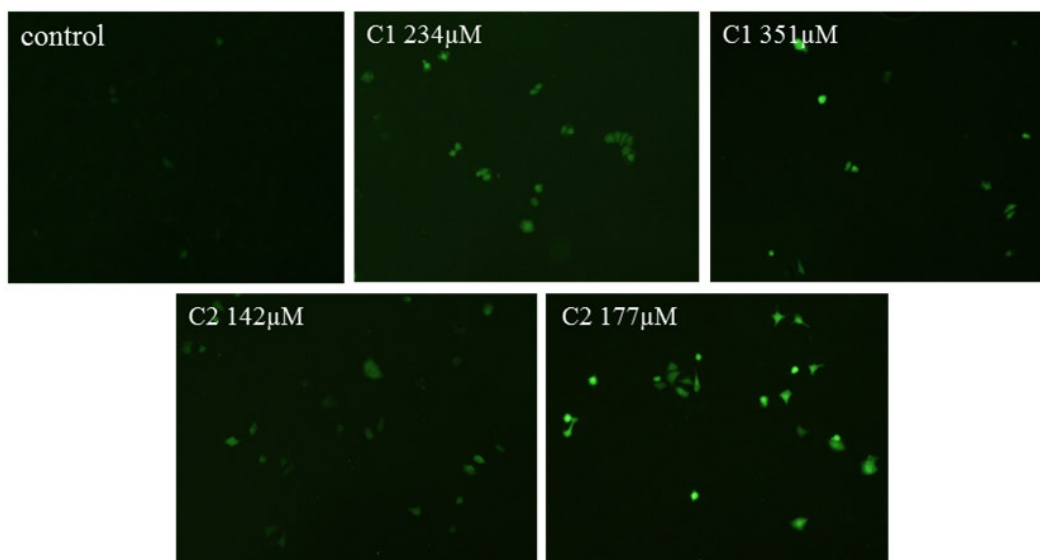


Fig. 6.

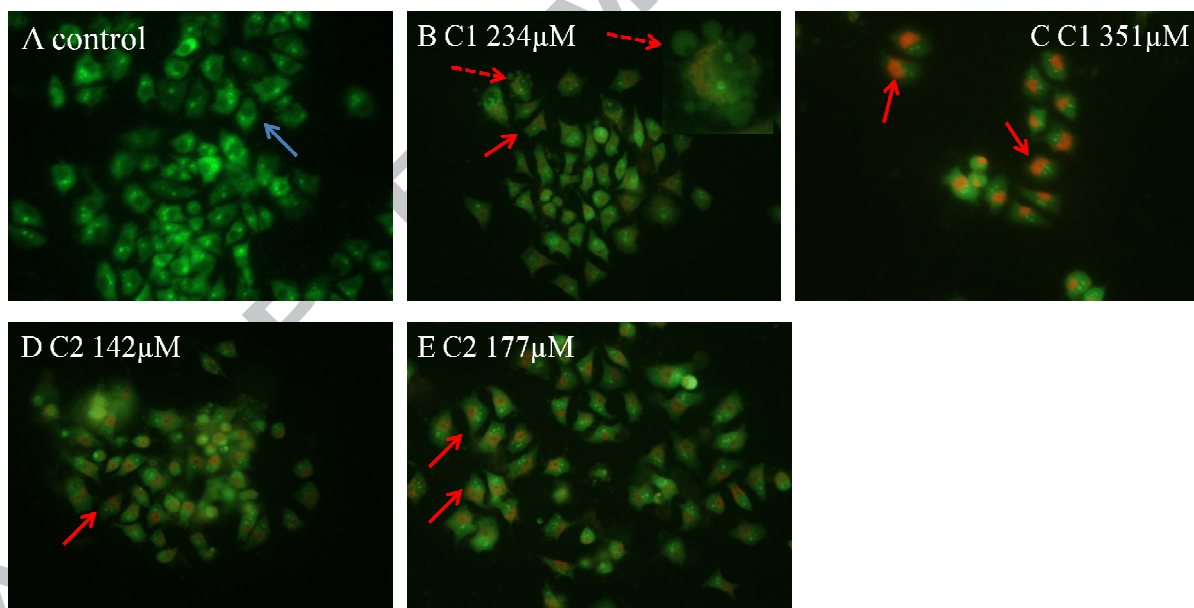


Fig. 7.

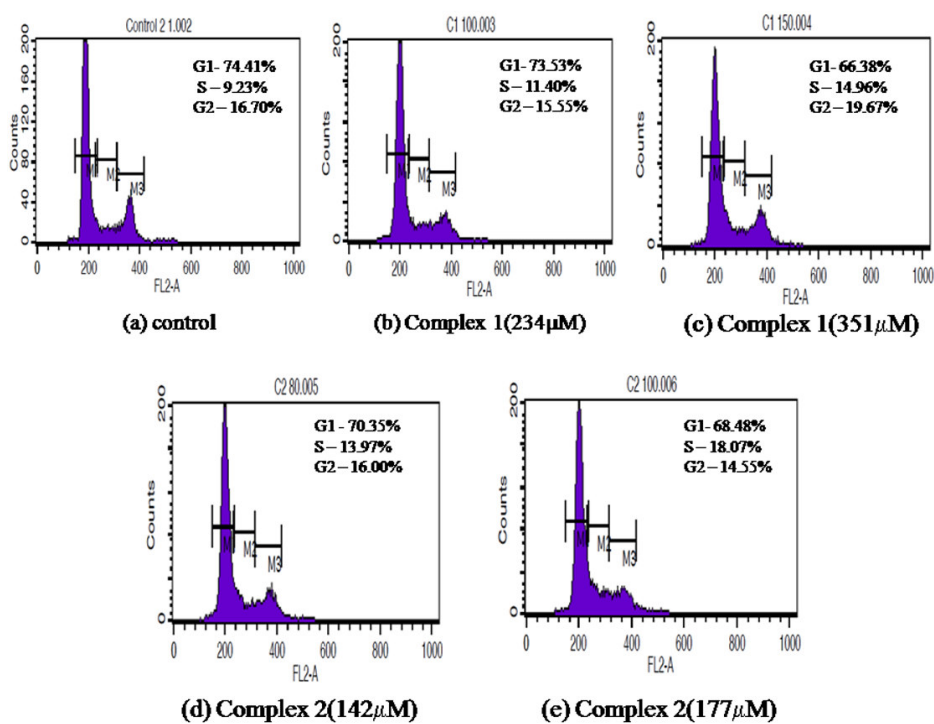
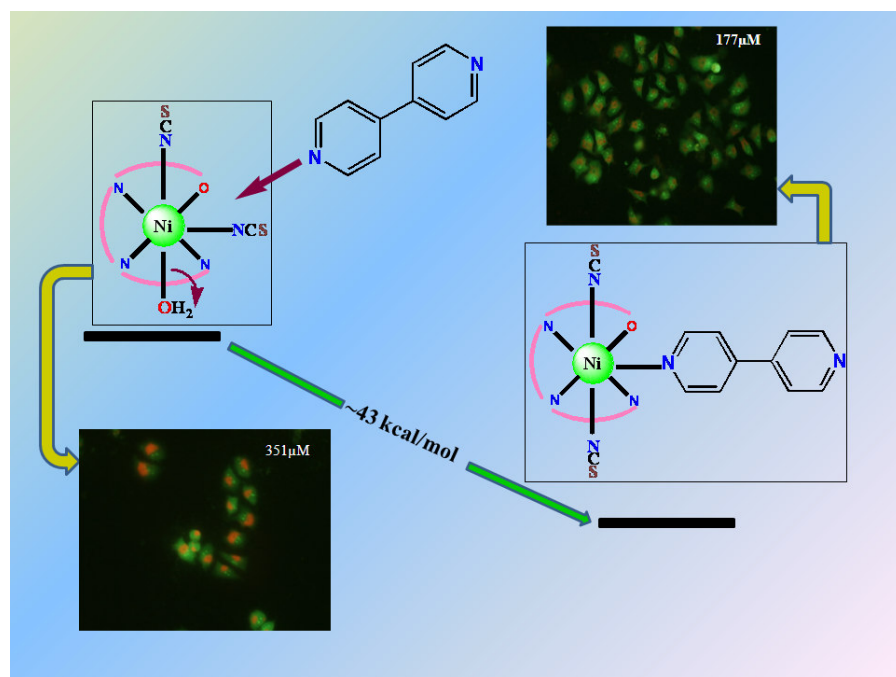


Fig. 8.

## Graphical Abstract



Addition of 4,4'-bipyridine as a neutral linker initiates a change in orientation of the thiocyanato ligands from *cis* in the parent species to *trans* in the product, instead of generating polynuclear species. The reaction pathway has been monitored experimentally and supported by DFT calculation. A bio-activity study reveals that the *trans* species has a higher antitumor activity than the *cis* species.

Synopsis

ACCEPTED MANUSCRIPT